Density mismatch in thin diblock copolymer films

S. Martins,[1] W. A. M. Morgado,[1] M. S. O. Massunaga,[2] and M. Bahiana[1]
[1]*Instituto de Física, UFRJ, Caixa Postal 68528, 21945-970 Rio de Janeiro, RJ, Brazil*
[2]*Laboratório de Ciências Físicas, Universidade Estadual do Norte Fluminense, Avenida Alberto Lamego 2000, 28015-620 Campos dos Goytacazes, RJ, Brazil*
(Received 19 April 1999; revised manuscript received 6 December 1999)

Thin films of diblock copolymer subject to gravitational field are simulated by means of a cell dynamical system model. The difference in density of the two sides of the molecule and the presence of the field causes the formation of lamellar patterns with orientation parallel to the confining walls even when they are neutral. The concentration profile of those films is analyzed in the weak segregation regime and a functional form for the profile is proposed.

PACS number(s): 61.41.+e, 64.60.Cn, 64.75.+g

I. INTRODUCTION

Recently, there has been a great deal of interest in studying the properties of thin films of diblock copolymers (DBCP) mostly because films of micro phase separated DBCP have been used for the fabrication of templates in a nanometer scale [1–3]. Apart from technological applications, it is important to understand the pattern formation in confined films of DBCP since it involves problems not present in bulk systems. Special attention has been given to interaction of the confining walls and each part of the molecule, since this effect determines the orientation of the microdomains. This issue has been addressed both theoretically [4–7] and experimentally [8–10] and the basic conclusions for the lamellar pattern are that, when the confining walls are neutral, the equilibrium pattern corresponds to lamellae perpendicular to the walls and, when the substrate prefers one kind of monomer, the pattern may consist of lamellae parallel or perpendicular to the walls, depending on the relation between the film thickness and the bulk lamellar width. The latter effect appears because the finiteness of the system brings about frustration and one has to take into account the amount of compression or stretching of the molecules in order to accommodate a certain number of lamellae between the two rigid walls.

One issue that has not been emphasized in the above studies is the possibility of density mismatch between the two parts of the molecules. At the bottom wall, as the denser part of the molecule sinks, lamellae parallel to the walls will form, even if the walls are neutral [11,12]. Being a bulk effect, the interaction with the gravitational field is capable of changing the microphase separation, even for infinite systems, as the lamellae tend to be aligned with the field far from the boundaries [11]. In finite systems, the lamellae perpendicular to the field present more diffuse interfaces and the gravitational field may completely destroy the microphase separation [12]. In the present paper, we consider this problem on two-dimensional films of even DBCP molecules as we analyze the effects of the degree of polymerization and film thickness on frustration by means of a cell dynamical system (CDS) model. We simulate films both in the weak- and strong-segregation regimes [(WSR)and (SSR)]. For the WSR, we empirically find the one-dimensional concentration profile and study the distortion of each layer within the lamellae.

In Sec. II, we define the model and outline the numerical scheme. Results for neutral and interacting walls in the presence and absence of the gravitational field are discussed in Sec. III. The effects of frustration are analyzed as they affect not only the size and number of lamellae, but also their internal structure. Also in this section we write the model parameters in terms of fundamental quantities and estimate their values for a typical experimental setting. In Sec. IV, the main conclusions are summarized.

II. COMPUTATIONAL MODEL

Block copolymers are linear-chain molecules consisting of two subchains A and B grafted covalently to each other. Below some critical temperature T_c, these two blocks tend to separate, but due to the covalent bond, they can segregate at best locally to form periodic structures [2]. Here, we consider only the case of even molecules corresponding to lamellar equilibrium patterns. CDS models have been successfully used in several problems of phase separation dynamics due to their computational efficiency and versatility [13–18], so we prefer that method for the simulations. As usual, in this kind of description we assign a scalar variable $\psi(n,t)$ to each lattice site corresponding to the coarse-grained order parameter in the nth cell at time t (time here is defined as the number of iterations). This order parameter represents the difference $\psi_A - \psi_B$, where $\psi_A(\psi_B)$ is the local number density of $A(B)$. The ingredients for the time evolution of ψ are: local dynamics dictated by a function with two symmetric hyperbolic attractive fixed points, diffusive coupling with neighbors, stabilization of the homogeneous solution and conservation of ψ. For the present problem, we also add the interaction with the gravitational field and with the confining walls. The conservation, when an external field is present, must be imposed by considering the Kawasaki exchange dynamics explicitly. The detailed explanation of this model is found in Ref. [19] for spinodal decomposition. With this, we come to the final equation for a melt of even DBCP molecules:

$$\psi(n,t+1)=(1-\epsilon)\psi(n,t)+\langle\langle C\{n,j;\mathrm{sgn}[I(n,t)-I(j,t)]\}[I(n,t)-I(j,t)]\rangle\rangle, \quad (1)$$

where

$$I(n,t)\equiv \mathcal{A}\tanh[\psi(n,t)]-\psi(n,t)+D[\langle\langle\psi(n,t)\rangle\rangle-\psi(n,t)]+hn_z+V_s(n) \quad (2)$$

is essentially the chemical potential. $\langle\langle\star\rangle\rangle$ is the isotropic space average of $\star$, $\mathcal{A}$ is a measure of the quench depth, and D is the diffusion coefficient. The parameter $\epsilon>0$ appears in this model to stabilize the solution $\psi=0$ in the bulk, for $\epsilon=0$ we have a model for spinodal decomposition, in which the domains can grow without bound. Scaling arguments have proved that $\epsilon\sim N^{-2}$, where N is the polymerization index [20]. h is the strength of the gravitational interaction and includes the gravitational field (which we assume is in the z direction) and the density difference between the two parts of the molecule, and n_z is the z component of n. For molecules with matched densities we just take $h=0$. A possible interaction with the walls appears via the surface term $V_s(n)$. C is the collision coefficient given by: $C(i,j;\alpha)=[\psi_c+\alpha\psi(j)][\psi_c-\alpha\psi(i)]/\psi_c^2$, where $\pm\psi_c$ are the fixed points of $\mathcal{A}\tanh\psi-\psi$ for $\mathcal{A}>1$. For all the simulations we used the values $\mathcal{A}=1.2$ and $D=0.5$, and uniformly distributed random initial conditions. The gravitational field, when present, is parallel to the smaller dimension. The direction normal to the field will be called the x direction. We consider systems with periodic boundary conditions in the x direction and hard walls in the z direction, separated by a distance L_z. At the hard walls we impose no flux boundary conditions in the form: $[I(z+1)-I(z)]_{boundaries}=0$.

III. RESULTS

In order to understand the effect of confinement on the lamellae width, we must first determine its bulk value. For that matter, we ran simulations on 512×512 lattices with periodic boundary conditions for different values of ϵ, and $h=0$. The resulting isotropically striped pattern was then Fourier transformed, and the bulk lamellar width W_b was measured in a standard way. Defining one lamella as $ABBA$ we have

$$W_b=\frac{2\pi}{\langle k\rangle_{eq}}, \quad (3)$$

where

$$\langle k\rangle_{eq}=\frac{\int S(k,\infty)k\,dk}{\int S(k,\infty)}. \quad (4)$$

$S(k,\infty)$ is the circular average of the structure function $S(\mathbf{k},t)=|\psi(\mathbf{k},t)|^2$, calculated at large times, that is, when the value of $\langle k\rangle$ approaches a constant value.

Just to make sure that the bulk lamellar width as measured above was not affected by the interface bending of the disordered pattern, we also measured W_b in 32×128 systems with hard neutral walls and zero field, or matched densities. As expected the equilibrium configuration correspond to lamellae normal to the hard walls [7,10] as in Fig. 1(a). W_b was then measured using the one-dimensional structure function for each line and finally averaging along the z direction. The values of W_b found in both determinations agree, so we conclude that the excessive interface curving of the disordered pattern does not affect the lamellar width. Since the disordered patterns are easier to obtain, we will consider the lamellar width obtained from them as our bulk equilibrium value W_b.

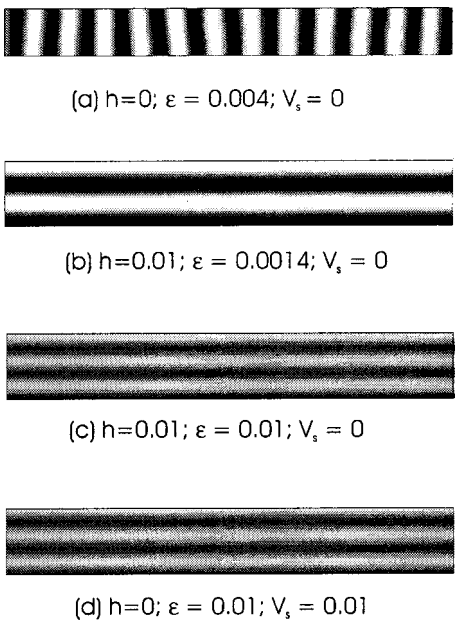

FIG. 1. Equilibrium patterns for confined films with $L_z=21$ and $L_x=256$ (only the first 150 columns are shown). (a) Neutral walls and matched densities. The lamellae are normal to the walls with the bulk periodicity. (b) Neutral walls and density mismatch, ϵ in the SSR. 1.5 lamellae are accommodated parallel to the walls. (c) Neutral walls and density mismatch, ϵ in the WSR. 2.5 lamellae are formed parallel to the walls. The lamellar width is 8.401, smaller then the bulk value of 9.422. (d) Interacting walls and matched densities, ϵ in the WSR. The lamellae are also parallel to the walls but are more segregated than in (c).

The results below correspond to simulations with $V_s=0$ (neutral walls), $h\neq0$ (mismatched densities), and $h=0$ (matched densities), and $V_s\neq0$ (interacting walls) and $h=0$. As will be seen, different patterns regarding the lamellae orientation appear: lamellae normal or parallel to the hard walls and a mixture of both.

A. Neutral walls

We focus now on films with mismatched densities ($h\neq0$), confined by neutral walls ($V_s=0$). In this situation, we observe patterns of lamellae parallel to the hard walls, or a mixture of wetting layers on the hard walls and lamellae normal to the walls in the center part of the film. First we analyze the case of lamellae parallel to the walls only. Due to the density difference of chains A and B, the denser part (say A) will be at the bottom, and the less dense part (say B), at the top. For a blend of two homopolymers A and B, the film would have the lower half filled with A and the upper one with B. The covalent bond between A and B parts hinders this complete separation and forces the alternation of A-rich

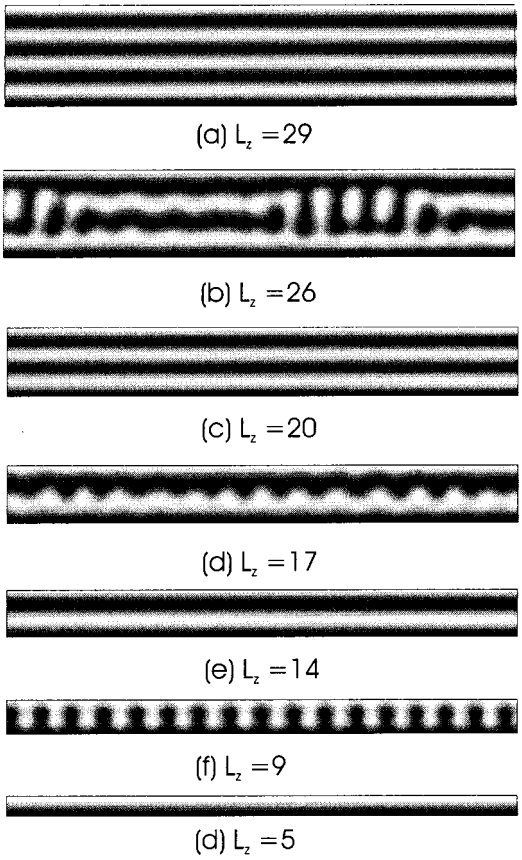

FIG. 2. Equilibrium patterns for films with $h=0.01$, $\epsilon=0.01$ (WSR), and variable width. $L_x=256$ but only the first 150 columns are shown. As the width L_z is decreased, the film goes discontinuously from $m=3$ to $m=0$ lamellar patterns. (b), (d), and (f) show transition patterns with mixed parallel and perpendicular lamellae.

and *B*-rich microregions that will then have thicker interfaces due to the interpenetration of domains [12]. In the extreme case, the existence of a density mismatch may completely destroy the segregation of *A* and *B*. The number of alternating lamellae will depend on both chain size, ϵ (see Fig. 1) and the separation between walls, L_z (see Fig. 2). Also, the equilibrium patterns will always have $m+1/2$ lamellae, where $m=0,1,2\ldots$.

As we vary L_z for a fixed ϵ we clearly see the effects of frustration. Figure 2 shows the transitions from $m=0$, to $m=1$, $m=2$, and $m=3$ patterns as L_z is changed from 5 to 29 for $\epsilon=0.01$ and $h=0.01$. The transition patterns are frustrated and present lamellae normal to the walls in the central region. Since full lamellar patterns are essentially one dimensional, we define the average concentration profile, $\langle\psi(n_z)\rangle_x$, as the average over the x direction of the vertical variation of ψ. Figure 3 shows the behavior of $\langle\psi(n_z)\rangle_x$, for three different situations, for now we are interested in Figs. 3(a) and 3(b) only. Figure 3(a) corresponds to the profile for $\epsilon=0.01$, $h=0.01$, $V_s=0$, and $L_z=21$. If we try to fit a sine function to that profile, we see that the fitting will miss only the wetting layers. From this we conclude that the system is in the WSR so that the inner layers can be described by just one Fourier component [21]. The wetting layers have an enhanced concentration due to gravitational field and the presence of the wall: the bottom and top *AB* layers are considerably stretched by the effect of buoyancy and do not

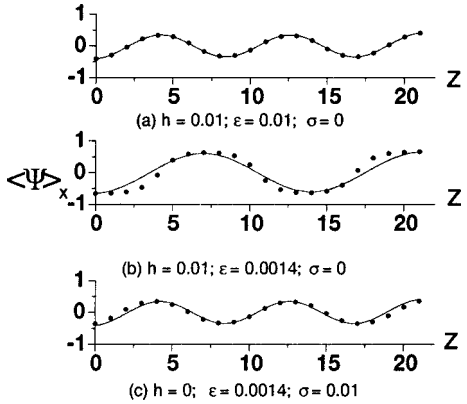

FIG. 3. Average concentration profiles for a film with $L_z=21$ and $L_x=256$. The continuous line corresponds to a fitting using Eq. (5). (a) Neutral walls, mismatched densities. The profile is well fitted by a sine function plus exponential enhancement at the hard walls. (b) Neutral walls, mismatched densities, and molecules larger than in (a). From the fitting it is clear that more than one Fourier component must be considered, indicating that the film is already in the SSR; (c) interacting walls $[V_s(1)=-\sigma=-V_s(L_z)]$ and matched densities.

experiment the penetration of other layers, resulting in an excess of *A* at the bottom and of *B* at the top.

A correction for this effect led us to the tentative function

$$\psi(x)=(-1)^{m+1}\eta\sin qx+2Ce^{-\beta L}\sinh 2\beta x \quad \text{for } -L/2\leqslant x\leqslant L/2, \tag{5}$$

which fits very well the profile in Fig. 3(a). For films in the WSR we found that the fitted value for q is indistinguishable from $2\pi(m+1/2)/L_z$, so we define the average lamellar width W, directly from the fitting, as $2\pi/q$. As will be seen below, the interaction with the gravitational field causes a distortion within the lamellae regarding the width of the *A* and *B*-rich layers, but, if considered as a unit, all the lamellae have a width very close to the average value. The transitions between consecutive values of m as we vary L_z is shown in Fig. 4. From this figure, we see that discontinuous transitions occur from a pattern in which the lamellae are stretched, compared to its bulk state, to a compressed state with one more lamella, as L_z is increased. The regions between steps of fixed m correspond to transition patterns in which lamellae normal to the walls form in the center portion of the film.

We can, alternatively, fix L_z and vary ϵ, which corresponds to fixing the film width and varying the bulk lamellae width. For $0.006<\epsilon<0.018$ we obtain patterns with $m=2$, in the range $0.004<\epsilon<0.006$ again we observe a transition pattern, and decreasing ϵ further we find that a $m=1$ pattern appears. Figure 5 shows patterns with $m=1$, $m=2$ and in the transition region. The analysis of the transitions in this case is more complicated since for $\epsilon<0.004$ the system is no longer in the WSR as can be seen from the fitting of Eq. (5) in Fig. 3(b). It is clear that other Fourier components need to be included in this case.

The accommodation of the lamellae distorts their widths nonuniformly as may be easily checked from the plot of the width of each individual *A*-rich and *B*-rich layer. Figure 6 shows the behavior, as a function of ϵ, of the widths of the

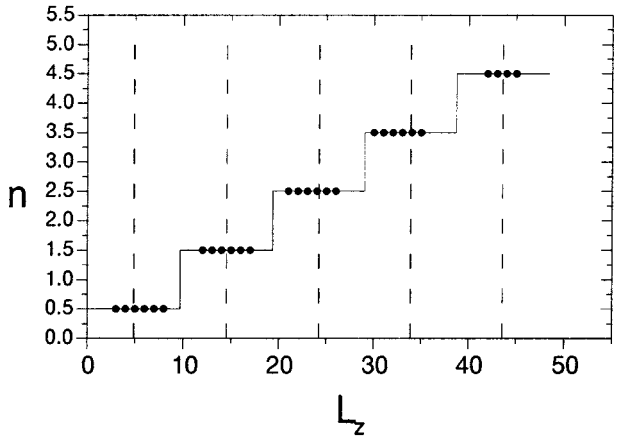

FIG. 4. Total number of lamellae, n, as a function of the film thickness L_z for a film with mismatched densities, confined by neutral walls. The solid points on the steps represent lamellar patterns with n lamellae parallel to the hard walls and between consecutive steps the film is in a mixed configuration with horizontal and vertical lamellae. The vertical dashed lines correspond to the film thickness adequate to accommodate the corresponding number of lamellae but with the bulk width W_b. We see that as the film width increases, discontinuous transitions between n stretched lamellae and $n+1$ compressed lamellae occur.

first A-rich layer that wets the bottom wall (w_1), the first B-rich layer connected to the bottom wetting layer (w_2), and one quart of the central lamella ($w_c = W/4$). For the sake of comparison, the variation of the bulk width, $w_b = W_b/4$, of A-rich (or B-rich) layers is also plotted. Although the variation is small compared to the bulk behavior, we see that $w_2 < w_c < w_1$ consistently. This happens because there is a reduction in the number of A and B contacts in the first layer (for the lack of neighboring molecules from below) and an increase in the next one because the gravitational field shifts the A parts downwards. As we separate the regions where the

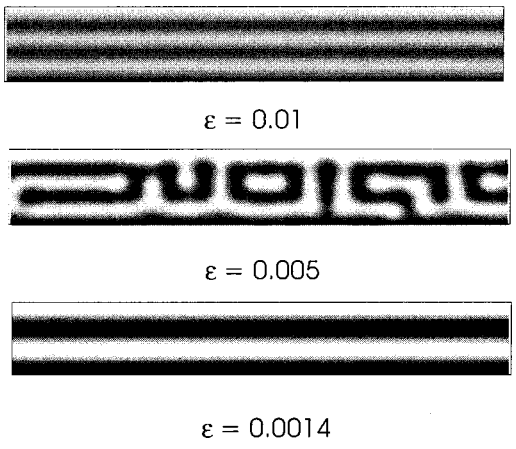

FIG. 5. Equilibrium patterns for confined films with $L_z = 21$ and $L_x = 256$ (only the first 150 columns are shown) three different values of ϵ. As in the case of variable film width, the number of lamellae varies discontinuously and transition patterns with mixed orientation lamellae appear. For $\epsilon = 0.01$ 2.5 weakly segregated lamellae are formed, the concentration profile can be well fitted by Eq. 5. $\epsilon = 0.005$ produces a transition pattern and $\epsilon = 0.0014$, a more segregated pattern with 1.5.

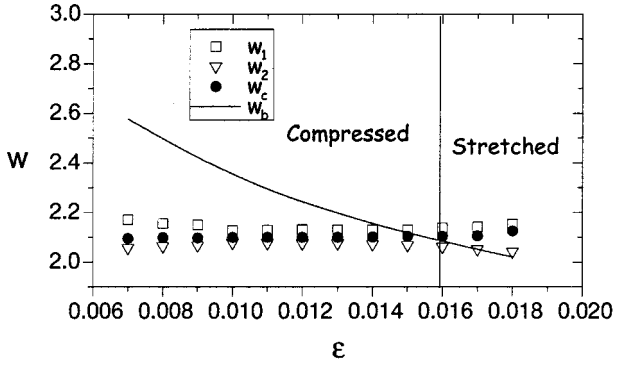

FIG. 6. Variation of A-rich and B-rich layers as a function of ϵ for films with 2.5 lamellae. w_1, w_2 are the widths of the lowest A-rich and B-rich layers, w_c is 1/4 of the central lamella and w_b is 1/4 of the bulk lamellar width. The vertical line indicates the separation between regions where the film is in compressed and stretched states. All the widths are measured in units of lattice spacings.

lamellae are compressed and stretched as compared to the bulk, we notice two different situations. In the compressed region, w_1 increases as N increases (ϵ decreases), due to a compression of the internal layers caused by the greater stretching of the surface layers which produces an increase in the internal pressure (for L_z fixed). We expected the inverse effect to happen when N was reduced in the stretched region: the internal layers would shrink producing a tension that would stretch the surface (larger effect) and second layers (smaller effect). But, in fact, we observe a drastic reduction of the second layer acting as a tension center for surface and central layers (Fig. 6).

It is clear that the above effects are meaningful only for thin films. The transition from this to the bulk behavior may be observed as we analyze w_1, w_2, and w_c as a function of the film thickness L_z. If the bulk behavior prevails, $w_2 \approx w_1 \approx w_2 \approx w_b \approx L_z/m$. As we increase L_z and observe films with increasing number of lamellae, we find $w_1 \rightarrow w_2 \rightarrow w_c \rightarrow w_b$. On the other hand, the slope α of each group of w values is proportional to $m^{-0.8}$ instead of m^{-1}, which reflects the different behavior of each layer of DBCP under stretching or compressions as can be seen in Fig. 7.

B. Interacting walls

The effect of surface fields in the formation of lamellar patterns has been extensively studied [4–10]. Our goal here is to compare the effect of the surface and bulk fields, so we first consider a film of DBCP molecules with matched densities confined by interacting walls in such a way that the bottom wall attracts the denser component and the top wall prefers the less dense component. As will be seen below, in many ways this choice of walls produces a pattern similar to the one obtained with neutral walls and a density mismatch, but the two situations are, in fact, different.

The above interaction with walls may be simulated by choosing the surface interaction as: $V_s = \sigma$ for $z = 1$ and $V_s = -\sigma$ for $z = L_z$. The equilibrium pattern obtained for $\epsilon = 0.01$, $L_z = 21$, $h = 0$, and $\sigma = 0.01$ is very similar to the one with the same values of ϵ and L_z, $\sigma = 0$, and $h = 0.01$, as both present 2.5 lamellae parallel to the walls (see Figs.

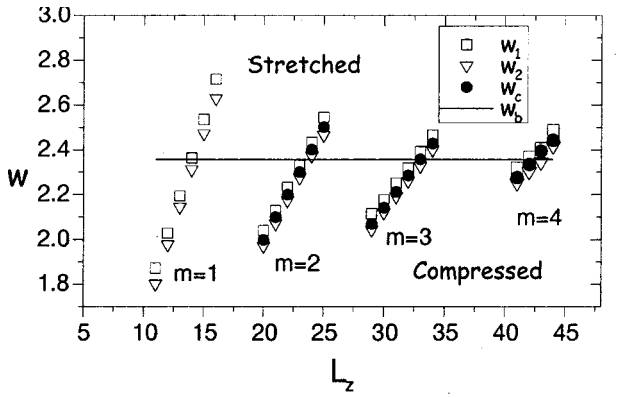

FIG. 7. Variation of *A*-rich and *B*-rich layers as a function of L_z for films with $\epsilon=0.01$. We use here the same notation of Fig. 6. Each group of points corresponds to lamellar patterns with $(m+1/2)$ lamellae. As L_z, and correspondingly m, increases, the film behaves more like a bulk sample in the sense that the distortion of lamellae is less significant. The slope α of each group is proportional to $m^{-0.8}$, for larger values of L_z a crossover to the bulk behavior $\alpha \propto m^{-1}$ is expected.

1(c) and 1(d), respectively). The first distinction appears in the segregation of domains: it is clear that the pattern in Fig. 1(c) is less segregated due to effect of interpenetration of domains driven by the gravitational field. A substantial difference appears for larger values of h and σ. Figure 8 shows patterns with the same value of $\epsilon=0.01$ and $L_z=21$ but one with surface field only and the other with density mismatch only. In this case, the lamellar structure still exists for $\sigma=0.04$ but here, for $h=\sigma$ the lamellar structure is completely destroyed in the center of the film.

C. Comparison with real systems

The parameters used so far are related qualitatively to actual quantities, $\mathcal{A}-1$ is a measure of the quench depth, for example, $\epsilon^{-1/2}$ is proportional to the polymerization index, and h combines the strength of the gravitational field and the density difference. To obtain meaningful values for the parameters, we must rescale our model equation in order to obtain the fundamental quantities. This is not straightforward

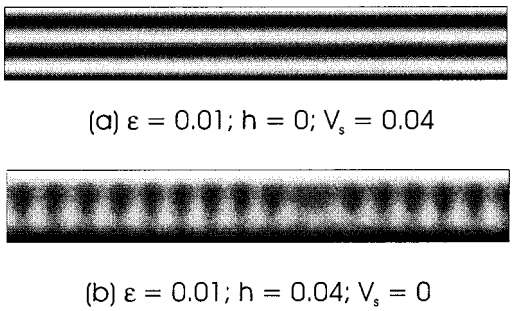

FIG. 8. A comparison between bulk and surface interactions. (a) Interacting walls and matched densities. Although the surface interaction is stronger than the one considered so far, the only noticeable difference is the segregation of the wetting lamellae. (b) Neutral walls and mismatched densities. Increasing the value of the bulk field h by the same amount as the surface field the observed pattern changes dramatically: instead of a lamellae pattern we observe a frustrated mixed orientation pattern.

since CDS modeling is discrete in its nature and the function dictating the dynamics is arbitrarily chosen. The purpose of this type of model is to give a description on a mesoscopic scale and has been very successful on this issue due to its computational efficiency that allows the exploration of asymptotic regimes of fairly large systems. But, still, we may at least estimate orders of magnitude by reading Eq. (1) as a crude discretization of a generalized Cahn-Hilliard equation. For small amplitudes of ψ we use [16,19,22]

$$\frac{\partial \psi}{\partial t}=\nabla^2\mu_0+h\nabla M\cdot\hat{\mathbf{z}}-\epsilon\psi. \tag{6}$$

The equation above results from writing the continuity equation with a ψ current defined in terms of the appropriate Landau-Ginzburg free-energy

$$\frac{F}{k_BT}=\int d^3r\left[-\frac{b}{2}\psi^2+\frac{u}{4}\psi^4+\frac{c}{2}(\nabla\psi)^2\right]-h\int d^3rz\psi + \frac{\epsilon}{4\pi}\int d^3rd^3r'\psi G(r,r')\psi'=F_0+F_g+F_c, \tag{7}$$

such that

$$\mu_0=\frac{\delta F_0}{\delta\psi}.$$

The mobility has the form $M=\bar{M}(1-\psi^2/\psi_c^2)$ with $\psi_c=\sqrt{b/u}$. In this light, the correspondence between simulation and free-energy parameters is: $b=1-\mathcal{A}\approx 0.2$, $u=\mathcal{A}/3\approx 0.4$, $c=D\approx 0.5$, and $h\approx 0.01$.

A more convenient form for Eq. (6) is obtained by choosing the natural density $(\psi_c=\sqrt{b/u})$ and length $(\xi=\sqrt{c/b})$ scales [23]. Using these scales, we are able to write a dimensionless equation of motion

$$\frac{\partial \psi}{\partial t}=\nabla^2(-\psi^2+\psi^4+\nabla^2\psi)-\eta\psi\nabla\psi\cdot\hat{\mathbf{z}}-\epsilon\psi. \tag{8}$$

The important factor η measures the relative intensity of the h field and, for the typical value of $h=0.01$ used in the simulations, is given by

$$\eta=\frac{h\xi}{b\psi_c}\approx 0.1. \tag{9}$$

We can evaluate the form for η given the density mismatch $\Delta\rho=\rho_A-\rho_B$ between the phases and the gravitational field g. The total gravitational energy corresponds to the integral of the local density $\rho(r)$

$$F_g=\int d^3r\rho(r)gz=\frac{(\rho_A-\rho_B)g}{2\psi_0}\int d^3rz\psi, \tag{10}$$

which, compared to the standard Landau-Ginzburg form, gives

$$h=\frac{(\rho_A-\rho_B)g}{2k_BT\psi_0}. \tag{11}$$

The above form for h can be rescaled [23] to a dimensionless form η_{exp} that should be compared with the values used in simulations

$$\eta_{exp} \approx 10.0 \left(\frac{\xi}{Nb} \right) \left(\frac{\xi^4 \Delta\rho g}{k_B T} \right). \tag{12}$$

Typical experimental settings [23] are: $N \approx 2{,}000$ is the polymerization number, $b \approx 20$ nm, $\xi \approx 20$ nm is the correlation length, $\Delta\rho \approx 0.5 \times 10^3$ kg/m^3 is the density mismatch, $g \approx 10$ m/s^2 and $T \approx 320$ K. Thus, $\eta_{exp} \approx 10^{-7} - 10^{-8}$, so that the value $\eta = 0.1$ used in the simulations do not correspond to the usual experimental conditions. The observation of gravitational effects might be within reach if we use powerful centrifugation devices (today's technology can reach over $100g$ per ton of material, with a possible 10^3 factor gain for smaller samples). Besides, if we work near the critical temperature, the critical fluctuations will enhance the gravitational flipping (via the ξ^5 term in h). It might be possible to obtain another 10^3 factor gain by bringing the system a few degrees from T_c.

It is also interesting to compare our parameters with the ones used in the simulations of surface-induced ordered DBCP samples by Brown and Chakrabarti [24]. In that paper the authors used a modified Cahn-Hilliard equation, integrated by an Euler scheme with a time interval $\delta t = 0.01$ and unit lattice spacing. The resulting equation is very similar to ours, and it is possible to find an equivalence from their values of σ and ϵ if we relate their lattice spacing to ours. In the following, we use the subscript BC to identify variables in the context of Ref. [24]. The first step is to compare the equilibrium patterns with similar bulk lengths $w_{BC} \approx w$. Knowing the lattice size in both cases (L and L_{BC}) and counting the number of lamellae, m and m_{BC} we find the relation between the lattice spacing a_{BC} and a. For example, for the pattern in Fig. 1(b) of Ref. [24], $L_{BC} = 128$ and $m_{BC} = 13.5$, considering that the lamellar width is not affected by frustration in this case, $w_{BC} = L_{BC}/m_{BC} = 9.48\ a_{BC}$. In our case, a pattern with $w = 9.48a$ would accommodate $m = 2.5$ lamellae in a $L = 24$ lattice, which implies $a \approx a_{BC}$. The discretization of the differential equations, and expansion of the $\tanh\psi$ near $\psi = 0$, lead to the following relation between model parameters

$$\frac{\epsilon}{\epsilon_{BC}} = \frac{\mathcal{A}-1}{2} \frac{a_{BC}^2}{a^2} = \frac{\mathcal{A}-1}{2}. \tag{13}$$

For $\mathcal{A} = 1.2$, $\epsilon_{BC} = 0.1 \Rightarrow \epsilon = 0.01$, which is used throughout this paper. Following the same reasoning, the intensity of the surface interaction are related as

$$\sigma = (\mathcal{A}-1)\sigma_{BC}. \tag{14}$$

In Ref. [24], the authors use $\sigma_{BC} = 0.4$, which corresponds to $\sigma \approx 0.1$ for $\mathcal{A} = 1.2$. The dimensionless surface field for typical experimental settings are in the range 10^{-1} to 10^{-2} [23], so both σ and σ_{BC} correspond to reasonable experimental values.

IV. CONCLUSIONS

We have studied the effects of surface and bulk gravitational fields coupled with hard wall restrictions on the lamellar pattern formation of diblock copolymer systems. We have found that the two are the predominant factors to determine the final equilibrium pattern: lamellae tend to form normal to the field and their number is determined by the ability of the system to resolve the frustration caused by the confinement. Unresolved patterns present a mixture of wetting lamellae normal to the field and lamellae parallel to the field in the central part of the film. The gravitational field also distorts the periodicity of the lamellar pattern. The bottom A layer is larger than it would be if placed in the central part of the film. On the other hand, the next B layer is narrower, in such a way that the first lamella, defined as the sequence $ABBA$, has a width very close to the central lamellae.

The average concentration profile in the WSR was well fitted by a trial function which consists of the superposition of a sinusoidal function, characteristic of the WSR, and exponential functions for the enhanced concentration of the wetting layers.

The comparison of the simulation parameters with those of a typical experimental setting showed that a realistic value of the parameter h that incorporates both the gravitational field and the density difference should be of order 10^{-7}. The same analysis for the surface fields yields values in the range $10^{-1} - 10^{-2}$. With this we conclude that the observation of the gravitational bulk effect is very difficult and the surface interaction will easily dominate for the usual experimental settings. The same situation holds for blends of polymers. The observation of a bulk gravitational-type interaction will require the use of an ultracentrifuge and temperatures close to the critical temperature for phase separation.

ACKNOWLEDGMENTS

This work was partially supported by the Brazilian agencies CNPq and Faperj.

[1] M. Park, Ch. Harrison, P. Chaikin, R.A. Register, and D.H. Adamson, Science **276**, 1401 (1997).
[2] F.S. Bates and G.H. Fredrickson, Phys. Today **52**, 2 (1999).
[3] Zh.-R. Chen, J.A. Kornfield, St.D. Smith, J.T. Grothaus, and M.M. Satkowski, Science **277**, 1248 (1997).
[4] M.S. Turner, Phys. Rev. Lett. **69**, 1788 (1992).
[5] M. Kikuchi and K. Binder, Europhys. Lett. **21**, 427 (1993).
[6] G. Brown and A. Chakrabarti, J. Chem. Phys. **102**, 1440 (1995).
[7] G.T. Pickett and A.C. Balazs, Macromolecules **30**, 3097 (1997).
[8] A. Menelle, T.P. Russell, S. Anastasiadis, S. K. Satija, and C. F. Majkrzak, Phys. Rev. Lett. **68**, 67 (1992).
[9] P. Lambooy, T.P. Russell, G.J. Kellogg, A.M. Mayes, P.D.

Gallagher, and S.K. Satija, Phys. Rev. Lett. **72**, 2899 (1994).
[10] G.J. Kellogg, D.G. Walton, A.M. Mayes, P. Lambooy, T.P. Russell, P.D. Gallagher, and S.K. Satija, Phys. Rev. Lett. **76**, 2503 (1996).
[11] M. Bahiana, Physica A **257**, 307 (1998).
[12] M. Bahiana and W.A.M. Morgado, Phys. Rev. E **58**, 4027 (1998).
[13] Y. Oono and S. Puri, Phys. Rev. Lett. **58**, 836 (1987).
[14] Y. Enomoto and K. Kawasaki, Mod. Phys. Lett. B **3**, 605 (1989).
[15] A. Chakrabarti and J.D. Gunton, Phys. Rev. B **37**, 3798 (1988).
[16] M. Bahiana and Y. Oono, Phys. Rev. A **41**, 6763 (1990).
[17] M. Mondello and N. Goldenfeld, Phys. Rev. A **42**, 5865 (1990).
[18] A. Shinozaki and Y. Oono, Phys. Rev. Lett. **66**, 173 (1991).
[19] K. Kitahara, Y. Oono, and D. Jasnow, Mod. Phys. Lett. B **2**, 765 (1988).
[20] Y. Oono and M. Bahiana, Phys. Rev. Lett. **61**, 1109 (1988).
[21] L. Leibler, Macromolecules **13**, 1602 (1980).
[22] C. Yeung, T. Rogers, A. Hernandez-Machado, and D. Jasnow, J. Stat. Phys. **66**, 1071 (1992).
[23] G. Krausch, E.J. Kramer, F. Bates, J.F. Marko, G. Brown, and A. Chakrabarti, Macromolecules **27**, 6768 (1994).
[24] G. Brown and A. Chakrabarti, J. Chem. Phys. **101**, 3310 (1994).